Pergamon

Int. J. Heat Mass Transfer. Vol. 39, No. 7, pp. 1463–1474, 1996

0017-9310/96 $15.00+0.00

0017-9310(95)00222-7

Radiative exchange between square parallel channels in a concentric monolith structure

D. J. WORTH,† A. SPENCE and P. I. CRUMPTON‡
School of Mathematical Sciences, University of Bath, Bath BA2 7AY, U.K.

and

S. T. KOLACZKOWSKI
School of Chemical Engineering, University of Bath, Bath BA2 7AY, U.K.

(*Received* 11 *January* 1994 *and in final form* 20 *March* 1995)

Abstract—The use of catalytic monoliths in high temperature combustion applications means that heat exchange by radiation plays an important role. Initially, this paper derives the system of integral equations that is used to model radiative exchange in a catalytic monolith with square or circular channels. Since the system is often coupled with a complex system of differential and algebraic equations that models channel interaction and other processes in the catalytic combustor, a simple approximation to the integral equations is introduced to make the problem tractable. The approximation technique is compared, first with the numerical solution of the integral equation for a cylindrical single channel, and second with published data for a simple cavity. The results of these two exercises show that the integral equation system and its approximation yield similar results to other workers and hence are appropriate for the modelling situation.

1. INTRODUCTION

As interest has increased in the use of catalytic monoliths in primary combustion processes to reduce emissions of oxides of nitrogen, NO_X [1–3], so too has the need for the mathematical modelling of these reactions. Throughout the literature the monolith configuration has been used in a variety of combustion applications ranging from established technology areas, e.g. as a catalytic convertor to applications in novel designs of catalytic gas turbine combustors. The monolith reactor consists of a large number of parallel channels (with thin walls), and resembles a honeycomb structure. Although the monolith can be fabricated with channels varying in size, cell density and shape, the square shaped channel is frequently encountered in the literature and in commercial application. The surfaces of the channels may be coated with a high surface area 'wash-coat' (e.g. γ-alumina) that contains the dispersed catalyst(s) and this is the place where the heterogeneous combustion reaction occurs. In order to successfully model the physicochemical processes taking place in a monolith reactor it is important to consider heat transfer by radiation and interacting effects, particularly when surface temperatures of the monolith are greater than 1000 K and could be as high as 1500 K. At these temperatures, heat transfer by radiation may be significant in the following situations:

(1) Heat transfer between a surface of the channel and the end faces of the monolith, see Fig. 2. In some cases this may be a neighbouring monolith, while in others it could be the wall of the duct for the gases, whose surface temperature could be substantially lower than that of the monolith.

(2) As reactions occur in the monolith an axial surface temperature profile will develop (in the direction of the gas flow) and heat exchange will occur between the adjacent surface elements in front of and behind the differential element modelled, see Fig. 2.

(3) If there are temperature gradients in the radial direction (i.e. between neighbouring channels) then heat exchange will occur between the opposite faces of the channels in the direction of the radial temperature gradient.

It is to cope with the situation described in (3) above that a multichannel model has been developed in order to model how channels interact with one another. As described in [4]:

This may arise (a) unintentionally, e.g. as a result of poor fuel and air mixing, see, for example [5], and subsequent fuel maldistribution into the monolith, or (b) intentionally, e.g. as a result of coating alternate channels with catalyst, for example [6]. In both of these examples, both gas and wall temperatures will differ between the neighbouring channels, resulting in heat transfer across the connecting wall and con-

† Currently at AEA Technology, Waste Environmental Group, Harwell, Oxon OX11 0RA, U.K. Author to whom correspondence should be addressed.

‡ Currently at Oxford University Computing Laboratory.

NOMENCLATURE

A	Radiation view factor (multichannel model)
A_c	Cross-sectional area of a channel [m^2]
C_p	Mean gas heat capacity [J mol^{-1} K^{-1}]
E	Radiation view factor (multichannel model)
F, dF	Radiation view factor
F_T	Total flow rate into a channel [mol s^{-1}]
h	**H** for single channel
h_O, h_A	Approximations to integral operators K_O, K_A
H	Matrix of integral operator approximations
K_O, K_A	Integral operators
K	View factor (single channel model)
K	Matrix of integral operators
L	Length of the monolith [m]
O	Radiation view factor (multichannel model)
Q	Heat lost by radiation [W]
q_O	Radiative heat loss for single channel model [W m^{-2}]
q_R	Radiative heat flux for web wall surface [W m^{-2}]
q_W	Radiative heat flux for ring wall surface [W m^{-2}]
$\mathbf{q}_I$	Vector of incoming radiative heat fluxes [W m^{-2}]
$\mathbf{q}_O$	Vector of outgoing radiative heat fluxes [W m^{-2}]
$\hat{\mathbf{q}}_O$	Approximation to $\mathbf{q}_O$
$\mathbf{q}_W$	Vector of radiative heat losses [W m^{-2}]
T_1	Black body temperature at entrance to monolith [K]
T_2	Black body temperature at exit of monolith [K]
T_R	Web wall temperature [K]
T_W	Ring wall temperature [K]
$\mathbf{T}_W$	Vector of wall surface temperatures [K]
x	Axial distance [m]
y	Non-dimensional radiative heat loss for single channel model
$\hat{y}$	Approximation to y
z	Axial distance [m].

Greek symbols

δ	Non-dimensional parameter
ε	Solid wall surface emissivity
ε_h	Apparent hemispherical emissivity for circular channel
θ	Non-dimensional temperature
λ	Channel width [m]
σ_E	Stefan–Boltzmann constant [W m^{-2} K^{-4}]
χ	Non-dimensional parameter.

Superscripts

r	Web wall surface
+	Outside ring surface
−	Inside ring surface.

Subscripts

i	ith channel.

sequential interactions. In case (b), this feature is exploited [6] to reduce surface temperatures in the active channels and also to provide a preheated fuel and air mixture to the next catalytic stage in the combustor. In case (a) however, higher values of inlet fuel concentration may result in the presence of 'hot zones', which, if not dissipated as a result of channel interactions, may cause catalyst/substrate damage. Obviously, in both of these examples, modelling has a role to play, aiding system design.

Although other workers, e.g. [7, 8] have derived expressions for radiant heat exchange in monoliths with square channels, they have not considered the problem of modelling non-adiabatic systems where heat exchange between individual channels may occur. The modelling of radiation is only one part of the reacting model of which an overview has already been presented [9]. The system consists of differential, algebraic and integral equations and requires solution of first order initial value problems and second order boundary value problems. The inclusion of radiation terms in the multichannel model results in a very complex system of equations to be solved. Faced with this challenge an approximation technique for the radiation terms has been developed and is described in this paper. This makes the problem tractable and also offers modellers the choice of using a faster method to solve the radiation equations in a single channel, when channel interaction is not considered important. This paper therefore gives details of the way heat transfer by radiation has been modelled using the techniques in [10] to give a system of coupled integral equations, and describes the techniques used in the solution of the these equations.

To set the scene for the development of the radiation equations, an outline is presented of the way in which a monolith with square shaped cells is modelled. Further details may be obtained from earlier publications [11, 12] on this theme. In summary, the physical form of the square lattice substrate of the monolith is transformed into an axisymmetric configuration. Thus it is conceptually possible just to consider a strip of N square cells in the radial direction (see Fig. 1). This reconfigured multichannel structure enables the modelling of situations where any combination of fuel, heat, and velocity may be maldistributed between the

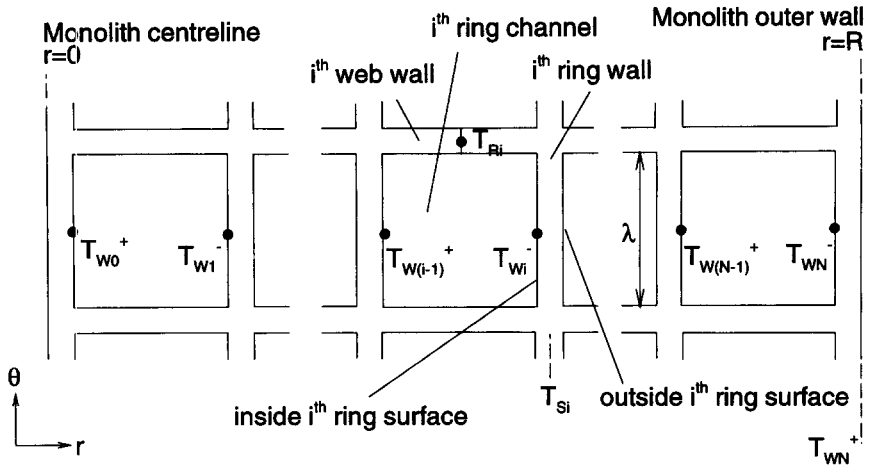

Fig. 1. Temperature variables in the multichannel structure.

channels. Further, the influence of external heating or cooling on channels internal to the monolith can also be investigated. The axisymmetry of the reconfigured system requires that no energy is transferred through web walls and so both web walls for each channel have the same temperature and hence only one web wall is considered. The model contains many parameters (e.g. length, channel diameter, thermal conductivity, emissivity) which can be varied to simulate different monolith structures and materials. The next section presents the steps in deriving the system of integral equations, Section 3 gives details of the approximation technique and its comparison with full numerical solution of the integral equation in the single channel case, and Section 4 compares predictions of energy fluxes from a cavity, calculated using the approximation technique with published data from [13].

2. MODELLING RADIATIVE HEAT EXCHANGE USING INTEGRAL EQUATIONS

In this section equations are derived for radiative heat exchange between channel wall surfaces and between the channel wall surfaces and the open end faces of the monolith. First, the various energy fluxes are defined and energy balance equations written in Section 2.1. Section 2.2 gives a general consideration of radiative heat transfer, and Section 2.3 applies this to a square channel to find an expression for the incoming energy flux to a wall surface. The balances of Section 2.1 are then used to derive the integral equations to be solved for the energy fluxes. This section is completed by deriving formulae for the view factors in a square channel in Section 2.4.

2.1. *General balance equations*

This section defines the energy fluxes to be considered and gives the overall energy balances which are a starting point for deriving the equations. For a wall surface at a distance x from the channel entrance let the heat loss via radiation, the outgoing and incoming heat fluxes, and the temperatures of the inside and outside ring surfaces and web walls (see Figs. 1 and 2) be denoted by the vectors

$$\mathbf{q}_{W_i}(x) = (q^-_{W_i}(x), q_{R_i}(x), q^+_{W_{i-1}}(x))^T$$

$$\mathbf{q}_{O_i}(x) = (q^-_{O_i}(x), q^r_{O_i}(x), q^+_{O_{i-1}}(x))^T$$

$$\mathbf{q}_{I_i}(x) = (q^-_{I_i}(x), q^r_{I_i}(x), q^+_{I_{i-1}}(x))^T$$

$$\mathbf{T}_{W_i}(x) = (T^-_{W_i}(x), T_{R_i}(x), T^+_{W_{i-1}}(x))^T$$

then the heat loss is the difference between the outgoing and incoming radiation

$$\mathbf{q}_{W_i}(x) = \mathbf{q}_{O_i}(x) - \mathbf{q}_{I_i}(x). \tag{1}$$

The walls are assumed to be diffuse and grey, thus the outgoing energy is the sum of the emitted energy and the incoming energy which is reflected, i.e.

$$\mathbf{q}_{O_i}(x) = \varepsilon\sigma_E \mathbf{T}^4_{W_i}(x) + (1-\varepsilon)\mathbf{q}_{I_i}(x). \tag{2}$$

Here ε is the emissivity of the coated wall and the assumption that the wall is grey means that reflectivity = 1 − emissivity, see ref. [10], p. 74. Eliminating $\mathbf{q}_{I_i}(x)$ between (1) and (2) gives

$$\mathbf{q}_{W_i}(x) = -\frac{\varepsilon}{(1-\varepsilon)}\{\mathbf{q}_{O_i}(x) - \sigma_E \mathbf{T}^4_{W_i}(x)\}. \tag{3}$$

An expression for $\mathbf{q}_{I_i}(x)$ in terms of $\mathbf{q}_{O_i}(x)$ is now sought which can be used in (2) to find the outgoing radiation which, in (3), will yield the radiation heat loss required for use in the model.

To find this relationship between incoming and outgoing radiation, consider as an example a differential element on an inside ring wall (see Fig. 2). Then the incoming radiation is made up of five parts (see Fig. 2):

two contributions, one from each end cavity

two contributions, one from each adjacent web wall and

one contribution from the opposite ring wall.

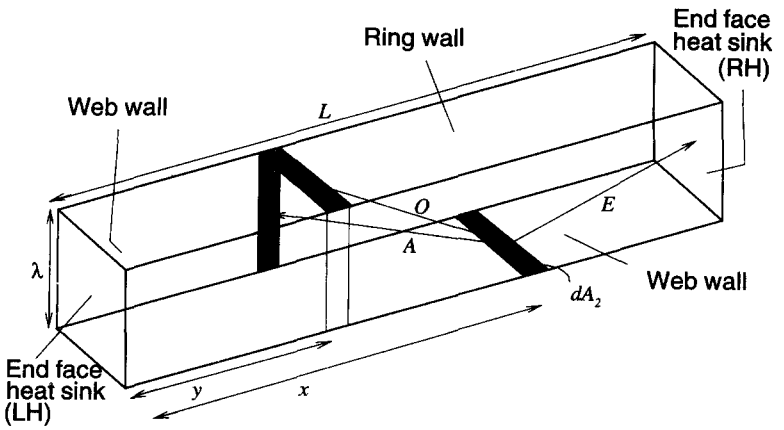

Fig. 2. View factor functions for a square channel.

2.2. *Heat exchange between a differential element and a finite area*

In this section the methods for the general calculation of heat interchange between surfaces classed as finite or differential are described (see [10]). These are used in Section 2.3 below to find the expression for the incoming radiation used in (2). The following explains how the individual heat fluxes can be calculated and shows which expression is used when considering heat exchange with the end faces and which when considering heat exchange with the channel walls.

First consider two differential areas dA_1 and dA_2 and a finite area A_2 (containing dA_2) which are arbitrary in space. Let dF_{d1-d2} be the fraction of energy leaving dA_1 arriving at dA_2 and F_{d1-2} be the fraction of energy leaving dA_1 arriving at A_2. Then

$$F_{d1-2} = \int_{A_2} dF_{d1-d2}$$

([10] equations in this reference are numbered 7–14). The reciprocity rule, used in the following form, gives the fraction of energy leaving A_2 arriving at dA_1:

$$F_{2-d1} = \frac{dA_1}{A_2} F_{d1-2}. \tag{4}$$

For one differential area (dA_1) and one finite area (A_2) the energy exchange from A_2 to dA_1 is

$$dQ_{2-d1} = q_{O_2} F_{2-d1} A_2$$

where q_{O_2} is the outgoing energy flux from A_2. So if q_{I_1} is the incoming energy flux to dA_1 from A_2, the following is obtained

$$q_{I_1} = \frac{dQ_{2-d1}}{dA_1} = q_{O_2} F_{2-d1} \frac{A_2}{dA_1} = q_{O_2} F_{d1-2}, \tag{5}$$

by (4). This expression is used to model radiation to the end cavities which are considered finite areas with a given temperature.

Now for two differential areas, the energy exchange from dA_2 to dA_1 is

$$d^2 Q_{d2-d1} = q_{O_2} dF_{d2-d1} dA_2,$$

where q_{O_2} is the outgoing energy flux from dA_2. Let q_{I_1} be the incoming energy flux to dA_1 from dA_2, then

$$q_{I_1} = \frac{d^2 Q_{d2-d1}}{dA_1} = q_{O_2} dF_{d2-d1} \frac{dA_2}{dA_1}. \tag{6}$$

Using the reciprocity relation $dF_{d2-d1} dA_2 = dF_{d1-d2} dA_1$ and integrating over the emitting area, the expression obtained is

energy flux to differential area dA_1 from A_2

$$= \int_{A_2} q_{O_2} dF_{d1-d2}. \tag{7}$$

Since the heat flux from the walls is *dependent on axial distance*, the channel walls are considered as the sum of differential elements at given axial distances. Therefore (7) is used to model radiation from channel walls.

2.3. *Radiant heat exchange in a square channel*

The expressions from Section 2.2 are now applied in the square channel of Fig. 2 to calculate the incoming energy to a channel wall, $\mathbf{q}_{I_i}(x)$, which can then be used in (2) to calculate the outgoing energy $\mathbf{q}_{O_i}(x)$. The incoming heat flux for the differential element dA_2, at a distance x along the channel, is

$$\begin{aligned} q_{I_i}^-(x) &= \text{energy from entrance} \\ &\quad + \text{energy from exit} \\ &\quad + \text{energy from opposite channel wall} \\ &\quad + \text{energy from adjacent channel walls} \\ &= \sigma_E T_1^4 E\left(\frac{x}{\lambda}\right) + \sigma_E T_2^4 E\left(\frac{L}{\lambda} - \frac{x}{\lambda}\right) \\ &\quad + \int_0^{L/\lambda} q_{O_{i-1}}^+(z) O\left(\left|\frac{x}{\lambda} - \frac{z}{\lambda}\right|\right) d\left(\frac{z}{\lambda}\right) \\ &\quad + 2\int_0^{L/\lambda} q_{O_i}^-(z) A\left(\left|\frac{x}{\lambda} - \frac{z}{\lambda}\right|\right) d\left(\frac{z}{\lambda}\right) \end{aligned}$$

where $E(X)$, $O(X)$ and $A(X)$ ($X = x/\lambda$) are view factors which are derived in Section 2.4. This expression can then be used for the first component of the vector equation (2) to give an equation for $q^-_{O_w}$. Similar equations can be found for the radiation losses from the other walls and together they form a coupled system of Fredholm integral equations of the second kind. The system is:

Radiative heat transfer for inside ring wall

$$q^-_{O_i}(x) = 2(1-\varepsilon)\int_0^{L/\lambda} q^r_{O_i}(z)A\left(\left|\frac{x}{\lambda}-\frac{z}{\lambda}\right|\right)\mathrm{d}\left(\frac{z}{\lambda}\right) + (1-\varepsilon)\int_0^{L/\lambda} q^+_{O_{i-1}}(z)O\left(\left|\frac{x}{\lambda}-\frac{z}{\lambda}\right|\right)\mathrm{d}\left(\frac{z}{\lambda}\right) + \sigma_E\left\{(1-\varepsilon)\left[T_1^4 E\left(\frac{x}{\lambda}\right)+T_2^4 E\left(\frac{L}{\lambda}-\frac{x}{\lambda}\right)\right] + \varepsilon(T^-_{W_i}(x))^4\right\}$$

Radiative heat transfer for web wall

$$q^r_{O_i}(x) = (1-\varepsilon)\int_0^{L/\lambda} q^-_{O_i}(z)A\left(\left|\frac{x}{\lambda}-\frac{z}{\lambda}\right|\right)\mathrm{d}\left(\frac{z}{\lambda}\right) + (1-\varepsilon)\int_0^{L/\lambda} q^r_{O_i}(z)O\left(\left|\frac{x}{\lambda}-\frac{z}{\lambda}\right|\right)\mathrm{d}\left(\frac{z}{\lambda}\right) + (1-\varepsilon)\int_0^{L/\lambda} q^+_{O_{i-1}}(z)A\left(\left|\frac{x}{\lambda}-\frac{z}{\lambda}\right|\right)\mathrm{d}\left(\frac{z}{\lambda}\right) + \sigma_E\left\{(1-\varepsilon)\left[T_1^4 E\left(\frac{x}{\lambda}\right)+T_2^4 E\left(\frac{L}{\lambda}-\frac{x}{\lambda}\right)\right] + \varepsilon(T_{R_i}(x))^4\right\}$$

Radiative heat transfer for outside ring wall

$$q^+_{O_{i-1}}(x) = (1-\varepsilon)\int_0^{L/\lambda} q^-_{O_i}(z)O\left(\left|\frac{x}{\lambda}-\frac{z}{\lambda}\right|\right)\mathrm{d}\left(\frac{z}{\lambda}\right) + 2(1-\varepsilon)\int_0^{L/\lambda} q^r_{O_i}(z)A\left(\left|\frac{x}{\lambda}-\frac{z}{\lambda}\right|\right)\mathrm{d}\left(\frac{z}{\lambda}\right) + \sigma_E\left\{(1-\varepsilon)\left[T_1^4 E\left(\frac{x}{\lambda}\right)+T_2^4 E\left(\frac{L}{\lambda}-\frac{x}{\lambda}\right)\right] + \varepsilon(T^+_{W_{i-1}}(x))^4\right\}.$$

The solution of these equations for each channel then allows the calculation of the vector of heat losses $\mathbf{q}_{W_i}$ from (3) in the following manner:

$$q^-_{W_i}(x) = -\frac{\varepsilon}{(1-\varepsilon)}\{q^-_{O_i}(x)-\sigma_E(T^-_{W_i}(x))^4\}$$

$$q_{R_i}(x) = -\frac{\varepsilon}{(1-\varepsilon)}\{q^r_{O_i}(x)-\sigma_E(T_{R_i}(x))^4\}$$

$$q^+_{W_{i-1}}(x) = -\frac{\varepsilon}{(1-\varepsilon)}\{q^+_{O_{i-1}}(x)-\sigma_E(T^+_{W_{i-1}}(x))^4\}.$$

As an aid to later simplification of the system of integral equations to a finite dimensional system of linear algebraic equations, define the integral operators K_A and K_O by

$$(K_A q)(x) = \int_0^{L/\lambda} q(z)A\left(\left|\frac{x}{\lambda}-\frac{z}{\lambda}\right|\right)\mathrm{d}\left(\frac{z}{\lambda}\right) \tag{8}$$

$$(K_O q)(x) = \int_0^{L/\lambda} q(z)O\left(\left|\frac{x}{\lambda}-\frac{z}{\lambda}\right|\right)\mathrm{d}\left(\frac{z}{\lambda}\right). \tag{9}$$

Then the system of three coupled integral equations for $\mathbf{q}_{O_i}$ can be written as

$$[(\mathbf{I}-(1-\varepsilon)\mathbf{K})\mathbf{q}_{O_i}](x) = \mathbf{g}(x, \mathbf{T}_{W_i}) \tag{10}$$

where

$$\mathbf{K} = \begin{pmatrix} 0 & 2K_A & K_O \\ K_A & K_O & K_A \\ K_O & 2K_A & 0 \end{pmatrix}$$

and

$$\mathbf{g}(x, \mathbf{T}_{W_i}) = \varepsilon\sigma_E \mathbf{T}^4_{W_i}(x) + \left[(1-\varepsilon)\left\{\sigma_E \mathbf{T}_1^4 E\left(\frac{x}{\lambda}\right) + \sigma_E T_2^4 E\left(\frac{L}{\lambda}-\frac{x}{\lambda}\right)\right\}\right](1,1,1)^T.$$

This linear system is the key equation for the inclusion of radiation in the multichannel model. The solution $\mathbf{q}_{O_i}$ found from it can be used in (3) to find the energy loss by radiation which is used in the wall surface energy balances of the model.

If $\mathbf{T}_{W_i}$ were known then (10) could be viewed in isolation. The solution of this 3×3 system of integral equations for the multichannel model would clearly require a great deal of computational effort. In this case however, $\mathbf{T}_{W_i}$ is not known and so (10) is coupled to a system of differential and algebraic equations of heat and mass conservation which comprises 22 equations (see [9]). In addition to this, the situation is further complicated by the multichannel nature of this model which means that the coupled integral–differential–algebraic system is written for each channel, and the equations of neighbouring channels are also coupled.

An attempt to solve the 3×3 system of integral equations numerically will create a large time delay in the solution of the total model, thus a simplification of the linear system is needed. Such a simplification is presented in Section 3 to allow the radiation terms to be computed more easily. This makes inclusion of radiation into the multichannel model possible. Before this is described in detail the derivations of the view factors $E(X)$, $O(X)$ and $A(X)$ are given, followed by

the radiation integral equation for a single channel model.

2.4. *View factors* E(X), O(X) *and* A(X)

The view factors for a square channel are calculated here using view factor algebra and standard view factors from [10]. The bodies involved in these exchanges are shown in Fig. 2. $E(X)$ $(X = x/\lambda)$ is the view factor function from an end face to a differential strip on one monolith wall, a distance x from the face. Thus from [10] (Appendix C no. 9 with $a = \lambda, b = \lambda, c = x$):

$$E(X) = \frac{1}{\pi}\left\{\arctan\frac{1}{X} + \frac{X}{2}\ln\frac{X^2(X^2+2)}{(X^2+1)^2} - \frac{X}{(1+X^2)^{1/2}}\arctan\frac{1}{(1+X^2)^{1/2}}\right\}.$$

The view factors $O(X)$ and $A(X)$ describe the fraction of energy leaving differential elements on opposite and adjacent channel walls respectively which reaches the differential element considered (dA_2 in Fig. 2). The distance between the emitting and receiving differential elements is denoted x and again $X = x/\lambda$. Let S_1 denote the opposite channel wall to dA_2, dA_1 denote a differential element on this side, and choose dA_2 to be at the exit to the channel. Then, from [10] (Appendix C number 5 with $a = L, b = \lambda, c = \lambda$), we have,

$$F_{dA_2-S_1} = \frac{1}{\pi}\left\{\sqrt{2}\arctan\frac{(L/\lambda)}{\sqrt{2}} - \arctan\frac{L}{\lambda} + \frac{(L/\lambda)}{(1+(L/\lambda)^2)^{1/2}}\arctan\frac{1}{(1+(L/\lambda)^2)^{1/2}}\right\}.$$

Further it was noted in Section 2.2 that there is an integral relationship between finite-differential and differential–differential view factors which in this case gives

$$F_{dA_2-S_1} = \int_S dF_{dA_2-dA_1} = \int_0^L dF_{dA_2-dA_1}\left(\frac{x}{\lambda}\right). \tag{11}$$

Now define

$$F(X) = \frac{1}{\pi}\left\{\sqrt{2}\arctan\frac{X}{\sqrt{2}} - \arctan X + \frac{X}{(1+X^2)^{1/2}}\arctan\frac{1}{(1+X^2)^{1/2}}\right\}$$

and note that $F_{dA_2-S_1} = F(L/\lambda) - F(0)$. Thus the integrand in (11) (the required view factor) must be $F'(X)$, where $'$ denotes differentiation with respect to X. Hence

$$O(X) = F'(X) = \frac{1}{\pi}(1+X^2)^{-3/2}\arctan\frac{1}{(1+X^2)^{1/2}}.$$

In an enclosed system, view factors from any point of the system to the rest of the system sum to unity, thus

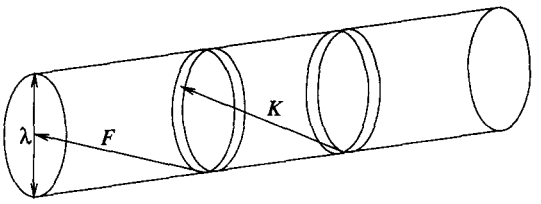

Fig. 3. The view factors for a cylindrical channel.

$$F_{dA_2-S_1} + 2F_{dA_2-S_2} + F_{dA_2-LH} + F_{dA_2-RH} = 1$$

or

$$F_{dA_2-S_2} = \tfrac{1}{2}\{1 - F_{dA_2-S_1} - F_{dA_2-LH} - F_{dA_2-RH}\}. \tag{12}$$

Here S_2 is the side adjacent to dA_2 and LH and RH are the entrance and exit of the channel, respectively. All the view factors on the right-hand side of (12) are known and so, assuming again that dA_2 is at the exit to the channel, the view factor of dA_2 from S_2 is

$$dF_{dA_2-S_2} = \frac{1}{2\pi}\left\{2\arctan\frac{L}{\lambda} - \sqrt{2}\arctan\frac{(L/\lambda)}{\sqrt{2}} - \frac{(L/\lambda)}{2}\ln\frac{(L/\lambda)^2((L/\lambda)^2+2)}{((L/\lambda)^2+1)^2}\right\}.$$

Arguing as for $O(X)$ above, it can now be shown that

$$A(X) = -\frac{1}{4\pi}\ln\frac{X^2(X^2+1)}{(X^2+1)^2}.$$

2.5. *Radiant heat exchange in a circular channel*

When channel interaction is not of interest it is only necessary to model one of the channels in the multichannel structure. It is common in the literature to consider circular channels in this case and to work with cylindrical coordinates. Thus, in this case, there is only one wall surface temperature profile to consider and hence only one integral equation to solve. This case is discussed for two reasons. First it is physically interesting in its own right and second it is used to check the validity of our approximation. The integral equation for radiative heat exchange can be derived in an exactly analogous way to that for the multichannel model described above. The view factor between the differential elements (now circular shaped rings on the channel wall) is $K(X)$ and $F(X)$ is the view factor from an end face to a differential ring on the channel wall (see Fig. 3). These view factors can be found in [10] (Appendix C nos. 29 and 30) and are given here for $X = x/\lambda$

$$K(X) = 1 - \frac{X(X^2+3/2)}{(X^2+1)^{3/2}}$$

and

$$F(X) = \frac{X^2+1/2}{(X^2+1)^{1/2}} - X.$$

The modelling approach of Section 2 is applied to a cylindrical channel and yields the integral equation

$$q_O(x)-(1-\varepsilon)\int_0^{L/\lambda} q_O(z)K\left(\left|\frac{x}{\lambda}-\frac{z}{\lambda}\right|\right)\mathrm{d}\left(\frac{z}{\lambda}\right)$$

$$=\sigma_E\left\{(1-\varepsilon)\left[T_1^4F\left(\frac{x}{\lambda}\right)+T_2^4F\left(\frac{L}{\lambda}-\frac{x}{\lambda}\right)\right]+\varepsilon T_W^4(x)\right\}$$

where q_O is the (dimensioned) outgoing heat flux, T_1 and T_2 are the upstream and downstream black body temperatures, respectively, and T_W is the wall temperature. The integral equation in non-dimensional form is

$$y(s)-(1-\varepsilon)\delta\int_0^1 y(t)K(\delta|s-t|)\,\mathrm{d}t$$

$$=\chi\{(1-\varepsilon)[\theta_1^4F(s\delta)+\theta_2^4F((1-s)\delta)]+\varepsilon\theta_W^4(s)\} \quad (13)$$

where y is the non-dimensional outgoing radiation flux, $s=x/\lambda$, $t=z/\lambda$, θ_1, θ_2 and θ_W are non-dimensional temperatures and δ and χ are non-dimensional parameters. For convenience later, denote the right-hand side of (13) by $f(s)$.

3. APPROXIMATION OF THE INTEGRAL EQUATION SYSTEM

As discussed at the end of Section 2.3 the motivation behind the search for an approximate solution strategy is that the cost of the full solution of the 3×3 system of integral equations (10) for the square geometry is likely to be very expensive even for one channel. The full solution would be accomplished by first discretising the channel at N points say. Then the system of integral equations (10) is replaced by a $3N\times3N$ linear system of algebraic equations. The solution of this system by Gaussian elimination requires $2(3N)^3/3$ floating point operations [14] (p. 99), and is repeated for every channel. Since N is likely to be very large this is a significant task. When coupled with the differential and algebraic equations in a multichannel model, the total cost for the solution process is very high.

In this section an approximation of the system of integral equations is described which relies on the very peaked nature of the kernels in the integral operators. This approximation

(i) eliminates the need for the full solution of the discretised, coupled integral equations,

(ii) dramatically reduces the time taken for solution of the problem and

(iii) is accurate enough for modelling purposes.

These features are described below as follows. The approximation is introduced heuristically for the square shaped channel in Section 3.1, and formulae for the new operator expressions are given in Section 3.2. In Section 3.3 the approximation is applied to a single cylindrical channel and Section 3.4 contains a brief but rigorous error analysis and a simple estimate for the error in the approximation obtained. This estimate is shown to be very accurate in the circular channel example (see Fig. 5). The final part of this section is a comparison between the approximate and numerical solutions of the integral equation for the cylindrical single channel model which demonstrates the accuracy of the approximation and supports the error analysis of Section 3.4.

3.1. *Integral approximation*

The key to this approximation is in the nature of the kernel functions $O(|x-z|/\lambda)$ and $A(|x-z|/\lambda)$ shown in Fig. 4 (for $L=60$). It is seen that the kernels are essentially zero over most of the interval, but over a small part they are very peaked. In a very loose sense these kernels resemble the delta function and so it is reasonable to make the approximation

$$\int_0^{L/\lambda} q(z)A\left(\left|\frac{x}{\lambda}-\frac{z}{\lambda}\right|\right)\mathrm{d}\left(\frac{z}{\lambda}\right)$$

$$\approx q(x)\int_0^{L/\lambda} A\left(\left|\frac{x}{\lambda}-\frac{z}{\lambda}\right|\right)\mathrm{d}\left(\frac{z}{\lambda}\right).$$

Denote the integral on the right hand side of this expression by $h_A(x)$, that is

$$h_A(x)=\int_0^{L/\lambda} A\left(\left|\frac{x}{\lambda}-\frac{z}{\lambda}\right|\right)\mathrm{d}\left(\frac{z}{\lambda}\right)$$

and hence, using the notation of (8),

$$(K_Aq)(x)\approx q(x)h_A(x). \quad (14)$$

Similarly, using the notation of (9)

$$(K_Oq)(x)\approx q(x)h_O(x) \quad (15)$$

where

$$h_O(x)=\int_0^{L/\lambda} O\left(\left|\frac{x}{\lambda}-\frac{z}{\lambda}\right|\right)\mathrm{d}\left(\frac{z}{\lambda}\right).$$

This development is very heuristic, but a straightforward error analysis which indicates that this approach does provide an acceptable approximation is given in Section 3.4 for the cylindrical channel.

The system of integral equations (10) is now replaced by a linear system of algebraic equations using the approximations for K_Aq and K_Oq in (14) and (15). To be precise define

$$\mathbf{H}(x)=\begin{pmatrix}0 & 2h_A & h_O\\ h_A & h_O & h_A\\ h_O & 2h_A & 0\end{pmatrix}$$

and then (10) is replaced by

$$(\mathbf{I}-(1-\varepsilon)\mathbf{H}(x))\hat{\mathbf{q}}_{O_i}(x)=\mathbf{g}(x,\mathbf{T}_{W_i}). \quad (16)$$

The solution $\hat{\mathbf{q}}_{O_i}(x)$ of this system is an approximation to the true solution of (10), $\mathbf{q}_{O_i}(x)$. The important point is that, for a fixed x, $\hat{\mathbf{q}}_{O_i}(x)$ is found by solving a 3×3 *algebraic* system. In comparison, the integral

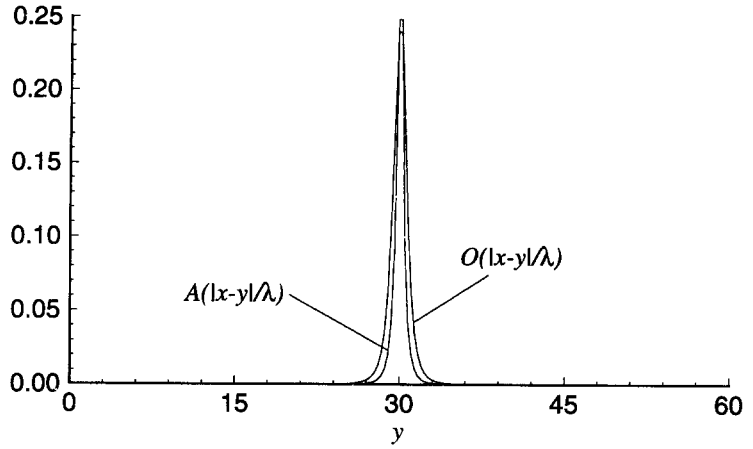

Fig. 4. The kernels $A(|x-z|/\lambda)$ and $O(|x-z|/\lambda)$ for $L = 60$, $\lambda = 1$, $x = 30$.

equation nature of (10) means that $\mathbf{q}_{O_1}(x)$ cannot be found easily as it depends on $\mathbf{q}_{O_1}(z)$ which appears in the integrals on the left-hand side of (10) for all $0 \leqslant z \leqslant 1$. (See the individual integral equations for each particular occurrence.)

The numerical effort to solve the radiation has decreased dramatically since (16) is merely a 3×3 linear system of algebraic equations to be solved now at each axial point of the discretisation. Thus for N discretisation points only $O(N)$ operations are needed rather than $O(N^3)$ operations for full numerical solution of (10).

3.2. *Formulae for* $h_A(x)$ *and* $h_O(x)$

By considering the definition of $h_O(x)$ it can be seen that this function has a physical meaning, it is exactly the view factor from a differential element on one channel wall to the whole of the opposite wall. Thus by considering the opposite wall as two rectangular pieces joined at an axial distance x the view factor from the differential element to each of the opposite pieces can be calculated from [10] (Appendix C number 9 with $a = x$ or $L-x$, $b = c = \lambda$). Then $h_O(x)$ is the sum of these two terms, i.e.

$$h_O(x) = F\left(\frac{x}{\lambda}\right) + F\left(\frac{L-x}{\lambda}\right)$$

where

$$F(X) = \frac{1}{\pi}\left\{\sqrt{2}\arctan\frac{X}{\sqrt{2}} - \arctan X + \frac{X}{(1+X^2)^{1/2}}\arctan\frac{1}{(1+X^2)^{1/2}}\right\}$$

(as in Section 2.4) and $X = x/\lambda$.

Notice that $F(X)$ here is just $F_{dA_2-S_1}$ from Section 2.4 with L/λ replaced by X. Thus, to calculate $h_A(x)$ the expression for $F_{dA_2-S_2}$ from Section 2.4 with L/λ replaced by X, $G(X)$ say, is used in the same way as $F(X)$ for $h_O(x)$. This yields

$$h_A(x) = G\left(\frac{x}{\lambda}\right) + G\left(\frac{L-x}{\lambda}\right)$$

where

$$G(X) = \frac{1}{2\pi}\left\{2\arctan X - \sqrt{2}\arctan\frac{X}{\sqrt{2}} - \frac{X}{2}\ln\frac{X^2(X^2+2)}{(X^2+1)^2}\right\}$$

and $X = x/\lambda$.

The next subsection demonstrates the approximation technique applied to the single channel radiation equation, and following that, a mathematical error analysis is given.

3.3. *The single channel model radiation approximation*

For the cylindrical channel considered in the single channel model the approximate solution, $\hat{y}$, can be found from the corresponding version of (16) which turns out to be a *single* algebraic equation. The dimensional integral term is approximated as follows

$$\int_0^{L/\lambda} q(z)K\left(\left|\frac{x}{\lambda} - \frac{z}{\lambda}\right|\right)\mathrm{d}\left(\frac{z}{\lambda}\right) \approx q(x)\int_0^{L/\lambda} K\left(\left|\frac{x}{\lambda} - \frac{z}{\lambda}\right|\right)\mathrm{d}\left(\frac{z}{\lambda}\right).$$

Thus, by defining

$$h(x) = \int_0^{L/\lambda} K\left(\left|\frac{x}{\lambda} - \frac{z}{\lambda}\right|\right)\mathrm{d}\left(\frac{z}{\lambda}\right) = \delta\int_0^1 K(\delta|s-t|)\,\mathrm{d}t$$

$\hat{y}(s)$ (the non-dimensionalised heat loss) is found from the equation

$$(1-(1-\varepsilon)h(s))\hat{y}(s) = f(s). \qquad (17)$$

Now the formula for $h(x)$ is precisely the view factor from the inside cylindrical surface of the channel to a differential ring on the surface. Now, the algebra of

view factors states that the sum of view factors in a closed geometry is unity and so it is clear that

$$h(s) = 1 - F(\delta s) - F(\delta(1-s))$$

where $F(X)$ is defined in Section 2.5. Thus the approximation to the integral equation (13) yields a solution, $\hat{y}$, given by:

$$\hat{y}(s) = \frac{\chi\{(1-\varepsilon)[\theta_1^4 F(\delta s) + \theta_2^4 F(\delta(1-s))] + \varepsilon\theta_w^4(s)\}}{1-(1-\varepsilon)h(s)}.$$

3.4. *Error analysis of the approximation for the circular single channel*

To analyse the error made by approximating y to $\hat{y}$ observe that, with $f(s)$ representing the right-hand side of the integral equation (13)

$$\begin{aligned} y(s) &= f(s) + (1-\varepsilon)\delta \int_0^1 K(\delta|s-t|)y(t)\,dt \\ &= f(s) + (1-\varepsilon)\delta \int_0^1 K(\delta|s-t|)[y(s) \\ &\quad + y(t) - y(s)]\,dt \\ &= f(s) + (1-\varepsilon)h(s)y(s) + (1-\varepsilon)\delta \\ &\quad \times \int_0^1 K(\delta|s-t|)[y(t)-y(s)]\,dt. \end{aligned} \tag{18}$$

Now, rearranging (17), the approximation to the integral equation, gives

$$\hat{y}(s) = f(s) + (1-\varepsilon)h(s)\hat{y}(s). \tag{19}$$

It is clear from (18) that the approximation can also be found by neglecting the last term on the right-hand side. Thus the reason why the approximation method works is as follows. The integrand in the last term on the right-hand side is 'small' since the $y(t)-y(s)$ term helps to cancel the peak in the $K(\delta|s-t|)$ term when $t \approx s$.

To continue the error analysis, subtract (19) from (18) to find

$$y(s) - \hat{y}(s) = \frac{e(s)}{1-(1-\varepsilon)h(s)} \tag{20}$$

where

$$e(s) = (1-\varepsilon)\delta \int_0^1 K(\delta|s-t|)[y(t)-y(s)]\,dt. \tag{21}$$

This expression involves the unknown exact solution $y(s)$ of (13), but by replacing y in (21) by $\hat{y}$, an approximation to $e(s)$ may be calculated as

$$\hat{e}(s) = (1-\varepsilon)\delta \int_0^1 K(\delta|s-t|)[\hat{y}(t)-\hat{y}(s)]\,dt \tag{22}$$

and then

$$y(s) - \hat{y}(s) \approx \frac{\hat{e}(s)}{1-(1-\varepsilon)h(s)}. \tag{23}$$

This integral can be calculated numerically for $s \in [0, 1]$. For $\delta = 10$, $\varepsilon = 0.8$, $\chi = 1$, $\theta_1 = 0.75$, $\theta_2 = 1.25$, and $\theta_w(s) = 1.5$ the right-hand side of (23) can be calculated and the absolute value is plotted in Fig. 5, along with the relative error $|y-\hat{y}|/\hat{y}$. This demonstrates that the absolute and relative errors are small in the centre of the channel and rise at either end. Nonetheless the relative error is certainly within standard error tolerances. Further note the closeness of Fig. 5, an approximation to the absolute and relative errors in $\hat{y}(s)$, to Fig. 6, a plot of the accurate calculation of these errors (Fig. 7 overlays the relative errors from Figs. 5 and 6 to confirm this very close agreement). (Note the difference in vertical scales between Figs. 5 and 6, and Fig. 7.)

As mentioned in the previous paragraph, the accuracy of the approximation procedure can be further checked by comparing $\hat{y}$ with the numerical solution of the full integral equation (carried out as in [15] to an absolute tolerance of 0.5×10^{-3}). The difference in the solutions is shown in Fig. 6 for the parameter values given above. The graph affirms that the approximation is close to the solution of the full integral equation in the centre of the range and the larger differences at the end points are because of the radiation conditions which the approximate solution cannot take into account fully. This may be expected from the analysis in [16] which reveals that large gradients in y can dominate the error, $|y-\hat{y}|$, and these large gradients are typically found near the entrance and exit of the channel. In spite of this, the approximation technique only introduces an 'error' of (at most) 0.5% into the solution for the outgoing heat flux (see the relative error plot). This gives confidence that the application of this approximation technique to the square shaped cells in a multichannel system will provide satisfactory results.

The solution of equation (16) is used in (3) to give an approximate heat loss $\hat{\mathbf{q}}_{w_i}$ which appears in the energy balance equations of the multichannel model [9].

4. COMPARISON WITH A SIMPLIFIED CAVITY OPENING

Both the square shaped cell, multichannel radiation model described in Section 3, and the circular single channel model are run in simulation mode, and for a range of inlet conditions the heat loss by radiation from one of the end faces is calculated. Since the condition simulated does not include the addition of fuel, the heat lost from the monolith can only be taken from the gas phase. Thus the heat loss may be determined from the overall gas phase heat balance across the system, that is, for the gas temperature $T(x)$,

$$Q = F_T \bar{C}_p(T(L) - T(0)) \tag{24}$$

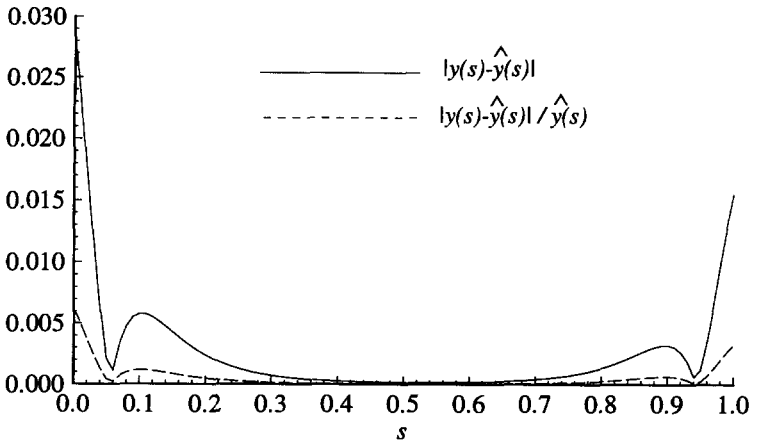

Fig. 5. Graph of absolute and relative errors caused by the approximation.

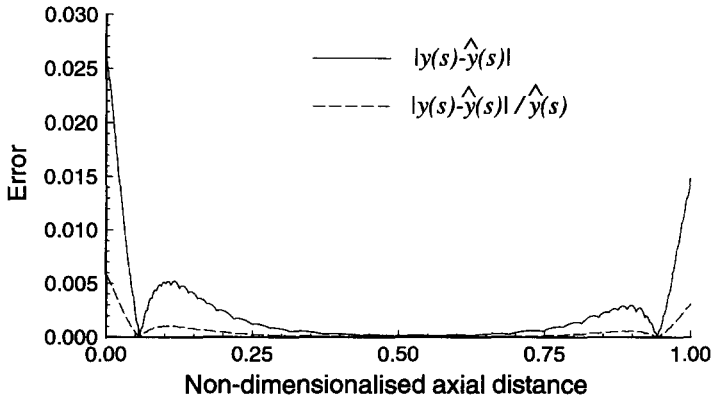

Fig. 6. Graph of $|y(s)-\hat{y}(s)|$ and $|y(s)-\hat{y}(s)|/\hat{y}(s)$.

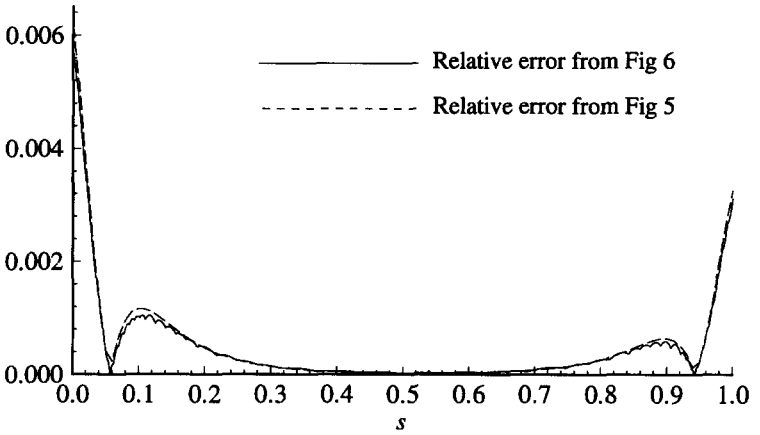

Fig. 7. Comparison of relative errors from Figs. 5 and 6.

where F_T is the total flow rate into a channel and $\bar{C}_p$ is a mean heat capacity for the gas. There is no net heat flux to the black body heat sink at the front face when the black body temperature (T_1) is set equal to the gas inlet temperature ($T(0)$) and this is the situation in these simulations. The results are compared with the solutions in [13] which are presented in graphical form for radiation from a circular hole of finite depth with diffuse reflecting walls at a constant temperature, T_W, say. For a fixed value of emissivity, ε, if the ratio L/λ of the cavity is greater than 3, the effective hemispherical emissivity approaches a limiting value, ε_h. In this application, since $L/\lambda \approx 100$, the heat loss, Q may be determined from

$$Q = \varepsilon_h A_c \sigma_E (T_W^4 - T_2^4)$$

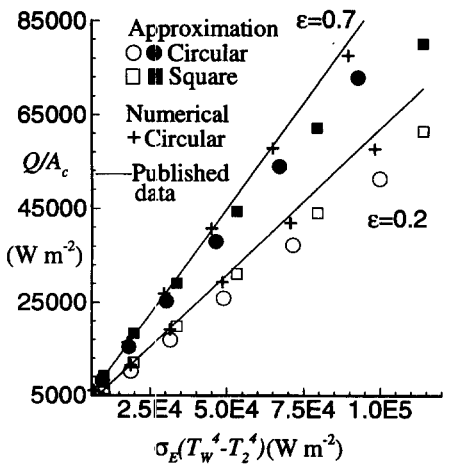

Fig. 8. Q/A_c against $\sigma_E(T_W^4 - T_2^4)$ for circular and square channels.

where A_c is the cross-sectional area of the cavity and T_2 is the downstream black body temperature.

Figure 8 plots Q/A_c against $\sigma_E(T_W^4 - T_2^4)$ for two values of ε. Here the heat loss Q is calculated from (24) and T_W is varied by varying the inlet temperature. The two values of ε chosen are 0.7 and 0.2 and the respective values of ε_h are 0.9 and 0.62. The value 0.7 is typical and may be used in simulations, the value 0.2 has been chosen only as a test. Agreement with the published results will place data points on the straight lines in Fig. 8.

In comparing the calculated data with the published data three points must be borne in mind:

(i) the published data is for circular channels only;
(ii) the wall temperature in the calculations was not flat as assumed in the published data and
(iii) a mean wall temperature must be used, which may be calculated in many ways.

Despite these differences it is clear from the figure that good agreement is obtained for both circular and square channels. The agreement deteriorates for higher wall energy fluxes (higher wall temperatures) due to the increasingly non-constant wall temperatures and thus a difficulty in deducing the correct mean wall temperature to use in the calculations. The data points lie below the lines of agreement because the approximate solution of the integral equation(s) does not take into account the total heat loss near the ends of the channels and so the wall temperature is higher than expected. Thus $\sigma_E(T_W^4 - T_2^4)$ has a high value, taking the data to the right of the straight lines. Data obtained when using the numerical solution of the integral equation for the circular channel is also plotted and lies close to the published data. These results verify the modelling of radiation in circular and square channels and give confidence in the use of the approximation technique for solving the system of integral equations when coupled with the differential and algebraic equations of the heat and mass balances.

5. CONCLUSIONS

A system of integral equations is developed for the modelling of radiative energy exchange in a square channel of a catalytic monolith reactor. Approximations to the integral operators are presented which allow the reduction of the integral equation system to a matrix system. This matrix system is solved to give the radiative fluxes which are then used in the coupled system of differential and algebraic equations that model the reaction in the monolith. For a circular channel the system becomes a single integral equation which can be solved numerically using the modified collocation approach of [15]. This was compared with the solution to the approximation of the integral equation and the two were found to agree well. Further, radiative flux data from a diffuse-grey cavity is compared with the fluxes predicted by both the single channel and multichannel equations. The comparisons were carried out at several different wall temperatures and the solutions of the equations presented here are a good match for the published data.

Acknowledgements—This paper reports some of the work on developing mathematical models of catalytic combustion systems for gas turbines which is funded under the DTI/SERC LINK scheme into New Catalysts and Catalytic Processes (Research grant no. GR/H00734).

REFERENCES

1. S. Blumrich and B. Engler, New developments in catalytic combustion for industrial gas turbines. In *Proceedings of the IMechE Conference on Combustion in Engines*, pp. 227–234. IMechE, Mechanical Engineering Publications Limited, London (1992).
2. A. K. Gupta and D. G. Lilley, Review: the environmental challenge of gas turbines, *J. Inst. Energy* **65**, 106–117 (1992).
3. Department of the Environment, A review of R&D on catalytic combustion, R&D Profile 38, Energy Efficiency Office, U.K. (June 1993).
4. S. T. Kolaczkowski and D. J. Worth, Modelling channel interactions in a non-adiabatic multichannel catalytic combustion reactor. In *Proceedings of the International Workshop on Catalytic Combustion* (Edited by H. Arai), pp. 100–103. Catalysis Society of Japan, Tokyo, Japan (1994).
5. W. S. Blazowski and D. E. Walsh, Catalytic combustion: an important consideration for future applications, *Combust. Sci. Technol.* **10**, 233–244 (1975).
6. R. A. Della Betta, N. Ezama, K. Tsurumi, J. C. Schlatter and S. G. Nickolas, Two stage process for combusting fuel mixtures, U.S. Patent, Ser. No. 618301, Pat. No. 5183401 (1993).
7. J. Sinkule and V. Hlaváček, Heat and mass transfer in monolithic honeycomb catalysts—III, *Chem. Engng Sci.* **33**, 839–845 (1978).
8. T. S. Ahn, Catalytic combustion of gas turbines, Ph.D. Thesis, University of New South Wales, Australia (1983).

9. D. J. Worth, S. T. Kolaczkowski and A. Spence, Modelling channel interaction in a catalytic monolith reactor, *Chem. Engng Res. Design* **71,** 331–333 (1993).
10. R. Siegel and J. R. Howell, *Thermal Radiation Heat Transfer* (2nd Edn). McGraw-Hill, New York (1981).
11. S. T. Kolaczkowski, P. I. Crumpton and A. Spence, Modelling of heat transfer in non-adiabatic monolith reactors, *Chem. Engng Sci.* **43,** 227–231 (1988).
12. S. T. Kolaczkowski, P. I. Crumpton, R. P. J. Lee and A. Spence, Channel interaction in a non-adiabatic monolith reactor, *Chem. Engng J.* **42,** 167–173 (1989).
13. S. H. Lin and E. M. Sparrow, Radiant interchange among curved specularly reflecting surfaces—application to cylindrical and conical cavities, *Trans. ASME, J. Heat Transfer* **82,** 299–307 (1965).
14. G. H. Golub and C. F. Van Loan, *Matrix Computations* (2nd Edn). Johns Hopkins University Press, Baltimore, MD (1989).
15. D. J. Worth, Mathematical modelling of a multichannel catalytic monolith combustor, Ph.D. Thesis, University of Bath, U.K. (1994).
16. P. I. Crumpton, Modelling of a non-adiabatic honeycomb reactor, Ph.D. Thesis, University of Bath, U.K. (1988).